J Solid State Electrochem (2010) 14:1227–1233
DOI 10.1007/s10008-009-0954-7

ORIGINAL PAPER

Determination of thermodynamic properties of $YRhO_3$(s) by solid-state electrochemical cell and differential scanning calorimeter

Aparna Banerjee · Ziley Singh

Received: 6 August 2009 / Revised: 5 October 2009 / Accepted: 7 October 2009 / Published online: 22 October 2009

Abstract The standard molar Gibbs free energy of formation of $YRhO_3$(s) has been determined using a solid-state electrochemical cell wherein calcia-stabilized zirconia was used as an electrolyte. The cell can be represented by: $(-)\mathrm{Pt}-\mathrm{Rh}/\{\mathrm{Y_2O_3(s)}+\mathrm{YRhO_3(s)}+\mathrm{Rh(s)}\}//\mathrm{CSZ}//\mathrm{O_2(p(O_2)}=21.21\ \mathrm{kPa})/\mathrm{Pt}-\mathrm{Rh}(+)$. The electromotive force was measured in the temperature range from 920.0 to 1,197.3 K. The standard molar Gibbs energy of the formation of $YRhO_3$(s) from elements in their standard state using this electrochemical cell has been calculated and can be represented by: $\Delta_f G^o\{\mathrm{YRhO_3(s)}\}/\mathrm{kJ\ mol^{-1}}(\pm 1.61) = -1,147.4 + 0.2815\ T\ (\mathrm{K})$. Standard molar heat capacity $C^o_{p,m}$ (T) of $YRhO_3$(s) was measured using a heat flux-type differential scanning calorimeter in two different temperature ranges from 127 to 299 K and 305 to 646 K. The heat capacity in the higher temperature range was fitted into a polynomial expression and can be represented by: $C^o_{p,m}(\mathrm{YRhO_3, s}, T)\left(\mathrm{J\ K^{-1}mol^{-1}}\right) = 109.838 + 23.318\times 10^{-3}\ T(\mathrm{K}) - 12.5964\times\ 10^5/T^2(\mathrm{K})$. $(305 \le T(\mathrm{K}) \le 646)$ The heat capacity of $YRhO_3$(s) was used along with the data obtained from the electrochemical cell to calculate the standard enthalpy and entropy of formation of the compound at 298.15 K.

A. Banerjee (✉) · Z. Singh
Product Development Division, RC & I Group,
Bhabha Atomic Research Centre,
Mumbai 400 085, India
e-mail: aparnab@barc.gov.in
e-mail: aparna_baner@yahoo.com

Keywords System Y–Rh–O · $YRhO_3$(s) · Gibbs free energy of formation · Enthalpy of formation · Heat capacity · Solid-state electrochemical technique · Thermodynamic functions

Introduction

Transition metal oxides of the 4d series are very interesting candidates for use as metallic conductors, catalysts [1, 2], and anode materials for photoelectrolytic cells [3]. Some rare earth orthorhodites act as semiconducting photocatalysts. Perovskite and spinel-type oxides of rhodium containing Rh^{+3} are good candidates for p-type wide gap semiconductors. Hence, these oxides have potential application in transparent oxide semiconductors [4]. Jarret et al. [5] have shown that orthorhodites of the distorted perovskite structure are semiconductors with a band gap of 2.2 eV. Rhodium superconducting compounds are also known [6].

Gysling et al. [7] have synthesized, characterized, and studied the catalytic properties of $LaRhO_3$(s) for conversion of syngas to linear alcohols. Ohta et al. [8] prepared rare earth (RE) orthorhodites, $RERhO_3$, by the solid-state reaction method and studied their crystallographic, magnetic, and electrical properties. Macquart et al. [9] have reported growth and characterization of single crystals of rare earth orthorhodites. Mizoguchi et al. [10] prepared several rhodium ternary oxides and determined their cell dimensions and stability in a reducing atmosphere. The orthorhodite $YRhO_3$(s) has an orthorhombic perovskite-type structure with space group Pbnm [11]. The tolerance factor t for $YRhO_3$ was calculated from the Goldschmidt's ionic radii of

Y^{+3}=1.019 Å, Rh^{+3}=0.665 Å, and O^{-2}=1.14 Å, and it was found to be 0.83 which matches with that of Cruickshank et al. [12, 13]. It is well known that the RhO_6 octahedron tilts when t is less than 0.9 and the perovskite structure-type ABO_3 transforms from a cubic to an orthorhombic structure as in the present case. Though magnetic and electrical properties of the orthorhodites have been studied, thermodynamic data like heat capacity, enthalpy of formation, and Gibbs free energy of formation are lacking in the literature. Hence, as part of systematic studies on the thermodynamic properties, measurements have been carried out on the Y–Rh–O system. A study of thermodynamic properties is essential for the optimization of synthesis parameters of rhodium compounds. This information is also important for the recovery of precious metals from scrap and from fission products. Phase diagrams of higher order containing these elements can be readily computed from thermodynamic data on ternary compounds [14].

In this study, $YRhO_3$(s) was synthesized and characterized by X-ray diffraction. Gibbs free energy of formation of the ternary oxide $YRhO_3$(s) was determined by using an electrochemical cell in the temperature range from 920.0 to 1,197.3 K. The heat capacity of $YRhO_3$(s) was measured in the temperature range from 127 to 646 K using a differential scanning calorimeter (DSC-131). Other thermodynamic parameters were evaluated from these experimental data.

Experimental

Materials

Rh_2O_3(s) was prepared from $RhCl_3$(s) (Johnson Matthey, England) by passing oxygen over $RhCl_3$(s) at 1,023 K. This gave α-Rh_2O_3(s), which on further heating at 1,273 K gave the β- phase [15]. $YRhO_3$(s), the ternary oxide in the Y–Rh–O system was prepared by the standard solid-state reaction technique. Y_2O_3(s) and Rh_2O_3(s) were mixed in stoichiometric proportions, pulverized thoroughly, and moistened with nitric acid fumed and heated to dryness. The sample was then reground and heated to 1,373 K in an evacuated quartz ampoule with intermediate grindings. The pellets were then gradually cooled to room temperature. $YRhO_3$(s) was characterized as a pure phase by X-ray diffraction technique. The values of interplanar spacing d obtained in the present study using STOE diffractometer with Cu-Kα radiation (λ=1.5406 Å) with Ni-filter and graphite monochromator is in good agreement with those reported in JCPDS number 34-1024 [11]. No impurity phase was observed in the X-ray diffraction pattern. The prepared sample was stored in a desiccator for heat capacity measurements. Preparative studies indicate a possible three phase field involving $YRhO_3$(s), Rh(s), and Y_2O_3(s). Hence, a phase mixture of {$YRhO_3$(s)+Rh(s)+Y_2O_3(s)} in the ratio 1:1:1 was made into a pellet of 10-mm diameter, 3-mm thickness, and at a pressure of 100 MPa, sintered in argon at 1,000 K, and used for electrochemical measurements.

The electrochemical cell assembly

A schematic diagram of the in-house fabricated experimental setup used for electrochemical measurements is shown in Fig. 1. A double compartment cell assembly with 0.15 mole fraction calcia-stabilized zirconia (CSZ) solid electrolyte tube with one end closed and flat was used to separate the gaseous environments of the two electrodes. Detailed experimental set up was described in an earlier publication [16]. The dimensions of the CSZ tube used were 13-mm outer diameter, 9-mm inner diameter, and 380 mm in length. The sample electrode, comprising of a mixture of {$YRhO_3$(s)+Rh(s)+Y_2O_3(s)} was pelletized and sintered as described earlier. Argon gas flowing at the rate of 1 dm^3h^{-1} was passed through towers containing molecular sieves and magnesium perchlorate to remove all traces of moisture. This served as the gaseous atmosphere for the cell compartment

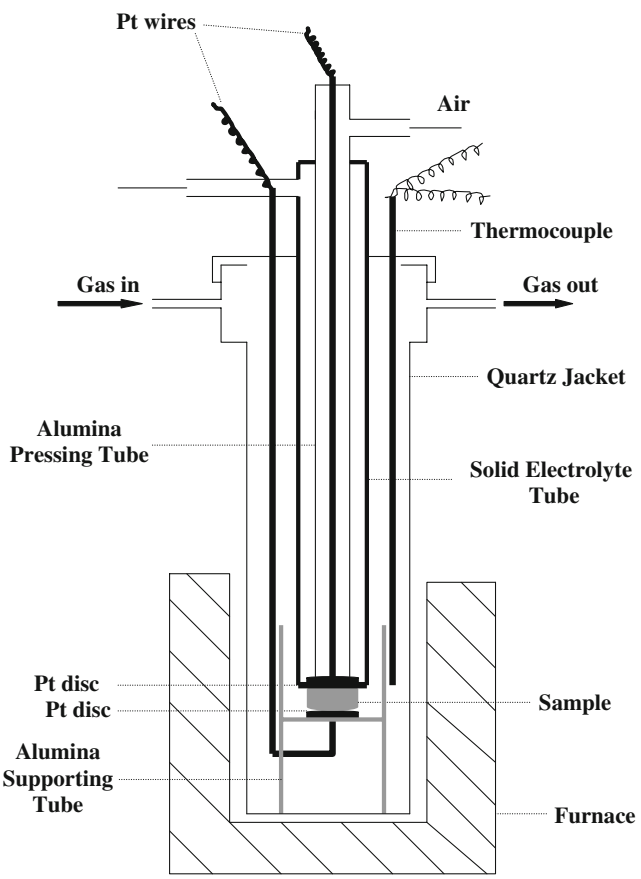

Fig. 1 Schematic diagram of the in-house fabricated experimental setup used for electrochemical measurements

containing the sample pellet. Air was used as the reference electrode. A Faraday cage was placed between the furnace and cell assembly. The cage was grounded to minimize induced electromotive force (e.m.f.). in the cell leads. Alumina sheathed Pt-40% Rh lead wires were used to measure the e.m.f. The temperature of the cell was measured by a calibrated chromel–alumel thermocouple located in the vicinity of the pellet. The e.m.f. of the cell was measured when the value of the e.m.f. was steady for 2–3 h using a high-impedance Keithley 614 electrometer. Voltages were reproducible in subsequent heating cycles. E.m.f. was measured after equilibrating the galvanic cells at 1,000 K for at least 24 h. The following cell configuration was employed in the present study:

$$(-)\mathrm{Pt-Rh}/\{\mathrm{YRhO_3(s)}+\mathrm{Y_2O_3(s)}+\mathrm{Rh(s)}\}\ //\mathrm{CSZ}//\mathrm{O_2}\{p(\mathrm{O_2})=21.21\ \mathrm{kPa}\}/\mathrm{Pt-Rh}(+) \quad (1)$$

The cell above is written in such a manner that the right hand electrode is positive. The reversibility of the solid-state electrochemical cell was checked by microcoulometric titration in both directions. A small quantity of current in microamperes was passed through the cell in either direction. Removal of the applied current returned the cell e.m.f. to its original value. The e.m.f. of the cell was also found to be independent of flow rate of the inert gas passing over the sample electrode. After electrochemical measurements, the X-ray diffraction pattern of the sample pellet did not reveal any new phase, indicating no chemical reaction either with the electrolyte tube or with the Pt-40% Rh lead wire.

Measurement of heat capacity of $YRhO_3$(s)

Heat capacity measurements were carried out using a heat flux-type differential scanning calorimeter (model: DSC-131, Setaram Instrumentation, France). The transducer of DSC-131 has been designed using the technology of the plate-shaped DSC rods made of chromel–costantan. It is arranged in a small furnace with a metal resistor of low-thermal inertia so as to produce high heating and cooling rates, thereby providing for high-speed experiments. The transducer also possesses very good sensitivity over the entire temperature range (100 to 650 K). The temperature calibration of the calorimeter was carried out in the present study by the phase transition temperature of National Institute of Standards and Technology (NIST) reference materials (mercury T_{fus}=234.316 K; gallium T_{fus}=302.914 K; indium T_{fus}=429.748 K; tin T_{fus}=505.078 K; lead T_{fus}=600.600 K) and AR grade samples (*n*-pentane T_{fus}=140.490 K; cyclohexane T_{fus}=280.1 K, T_{trs}=190.0 K; deionized water T_{fus}=273.160 K; potassium nitrate T_{fus}=400.850 K; silver sulfate T_{fus}=703.150 K). Heat calibration of the calorimeter was carried out from the enthalpies of transition of the reference materials. For the determination of heat capacity, NIST synthetic sapphire (SRM 720) in the powder form was used as the reference material [17]. Temperature calibration and experimental setup for the calorimeter have been described elsewhere [18]. Heat capacity of the oxide was determined in two different temperature ranges: (1) $127 \le T$ (K)≤ 299 and (2) $305 \le T$ (K)≤ 646.

The classical three-step method in the continuous heating mode was followed in this study to measure the specific heat in the first temperature range from 127 to 299 K. Heat flow as a function of temperature was measured at a heating rate of 5 K min^{-1} with high-purity helium as a carrier gas with a flow rate of 2 $dm^3 h^{-1}$. In order to determine heat capacity in the step-heating mode that is the second temperature range from 305 to 646 K, three sets of experiments were carried out in argon atmosphere at a heating rate of 5 K min^{-1} and a gas flow rate of 2 $dm^3 h^{-1}$. All three sets of experiments were performed under identical experimental conditions of heating rate, carrier gas flow rate, delay time, and temperature range. Two empty flat bottomed cylindrical aluminum crucibles with covering lids (capacity $10^{-4} dm^3$) of identical masses were selected for the sample and reference cells.

In the first run, both the sample and reference cells were loaded with empty aluminum crucibles. The heat flow versus temperature was measured at a heating rate of 5 K min^{-1}. In the second run, a known weight of NIST synthetic sapphire (SRM-720) was loaded in the sample cell keeping the crucible in the reference side empty, and once again, the heat flow versus temperature was measured in the same temperature range and at the same heating rate. In the third run, a known weight of the sample of $YRhO_3$(s) was loaded in the sample cell, reference cell being empty, and once again the heat flow as a function of temperature was measured. About 300–350 mg of the sample was used for the heat capacity measurements. In DSC-131, heat capacity of the sample under investigation can be calculated by a simple comparison of the heat flow rates in three runs as illustrated in the literature [19]. For a defined step of temperature, the thermal effect corresponding to the sample heating is integrated. Thermal equilibrium of the sample is reached after each step of temperature. If T_i represents the initial temperature, the temperature interval step is chosen between T_j and T_{j+1}; we define: $T_j = T_i + \Delta T$ and $T_{j+1} = T_i + (j+i)\,\Delta T$. The expression used for the calculation of heat capacity of the sample is given as:

$$C_p(T_j)_{\mathrm{sample}} = \langle(\mathrm{HF_{sample}} - \mathrm{HF_{blank}})\rangle / \langle(\mathrm{HF_{Ref}} - \mathrm{HF_{blank}})\rangle \times (M_{\mathrm{Ref}}/M_{\mathrm{sample}}) \times \left\langle C_{\mathrm{p}}(T_j)_{\mathrm{Ref}}\right\rangle \quad (2)$$

where HF_{blank}, HF_{Ref}, and HF_{sample} represent heat flow during first, second, and third runs, respectively. $C_p(T_j)_{sample}$

and $C_p(T_j)_{\mathrm{Ref}}$ represent the heat capacities of sample and reference material in joules per kelvin per gram, and M_{sample} and M_{Ref} represent the mass of sample and reference, respectively. The heat capacity, thus, obtained was then converted to joules per kelvin per mole. Accuracy of measurements were checked by measuring the specific heat of Fe_2O_3(s) (mass fraction 0.998) in the temperature range from 127 to 646 K, and the values were found to be within ±2% as compared with the literature values [20].

Results

Solid-state electrochemical measurements for the oxide cell

The e.m.f. of the solid state electrochemical cell is related to the partial pressure of oxygen at the two electrodes and is given by the relation:

$$E = (RT/nF)\int_{p'(\mathrm{O_2})}^{p''(\mathrm{O_2})} t(\mathrm{O^{2-}})\,\mathrm{d}\ln p(\mathrm{O_2}) \tag{3}$$

E is the measured e.m.f. of the cell, R=8.3144 $\mathrm{JK^{-1}mol^{-1}}$ is the universal gas constant, n is the number of electrons participating in the electrode reaction, F=96486.4 $\mathrm{Cmol^{-1}}$ is the Faraday constant, T is the absolute temperature, $t(\mathrm{O^{2-}})$ is the effective transference number of $\mathrm{O^{2-}}$ ion for the solid electrolyte, and $p''(\mathrm{O_2})$ and $p'(\mathrm{O_2})$ are the equilibrium oxygen partial pressures at the positive and negative electrodes, respectively. The transport number of oxygen ion in the present electrolyte cell arrangement is nearly unity ($t(\mathrm{O^{2-}})$>0.99) at the oxygen pressures and temperature range covered in this study. Hence, e.m.f. of the cell is directly proportional to logarithm of the ratio of partial pressures of oxygen at the electrodes:

$$E = (RT/nF)\ \ln\{p''(\mathrm{O_2})/p'(\mathrm{O_2})\} \tag{4}$$

Thus,

$$nFE = RT\ln p''(\mathrm{O_2}) - RT\ln\ p'(\mathrm{O_2}) \tag{5}$$

RTln $p''(\mathrm{O_2})$ is the oxygen chemical potential over the positive electrode and RTln $p'(\mathrm{O_2})$ is the oxygen chemical potential over the negative electrode. The solid-state electrochemical cell configuration is given in Eq. 1.

The half-cell reaction for the cell is given by:

$$3/2\ \mathrm{O_2(g)} + 6\ \mathrm{e^-} \rightarrow 3\ \mathrm{O^{2-}} \qquad \text{(at the cathode)} \tag{6}$$

and

$$\mathrm{Y_2O_3(s)} + 2\ \mathrm{Rh(s)} + 3\ \mathrm{O^{2-}} \rightarrow 2\ \mathrm{YRhO_3(s)} + 6\ \mathrm{e^-} \qquad \text{(at the anode)} \tag{7}$$

The overall cell reaction can be represented by:

$$\mathrm{Y_2O_3(s)} + 2\ \mathrm{Rh(s)} + 3/2\ \mathrm{O_2(g)} = 2\ \mathrm{YRhO_3(s)} \tag{8}$$

The least squares regression analysis of the e.m.f. gives:

$$E/\mathrm{V}(\pm 0.00165) = 0.6901 - 5.218\times 10^{-4}(T/\mathrm{K}) \qquad (920 < T/\mathrm{K} < 1197.3) \tag{9}$$

The uncertainties quoted are the standard deviation in e.m.f. The variation of e.m.f. as a function of temperature is presented in Fig. 2. The $\Delta_r G^o(T)$ for the reaction given in Eq. 8 involves the transfer of six electrons.

$$\Delta_r G^o(T) = -6\ FE = 2\ \Delta_f G^o\{\mathrm{YRhO_3(s)}\} - \Delta_f G^o\{\mathrm{Y_2O_3(s)}\} - 3/2\ RT\ln\ p(\mathrm{O_2}) \tag{10}$$

Substituting the value of $\Delta_f G^o\{\mathrm{Y_2O_3(s)}\}$ from the literature [21] and e.m.f. values from Eq. 9, the standard

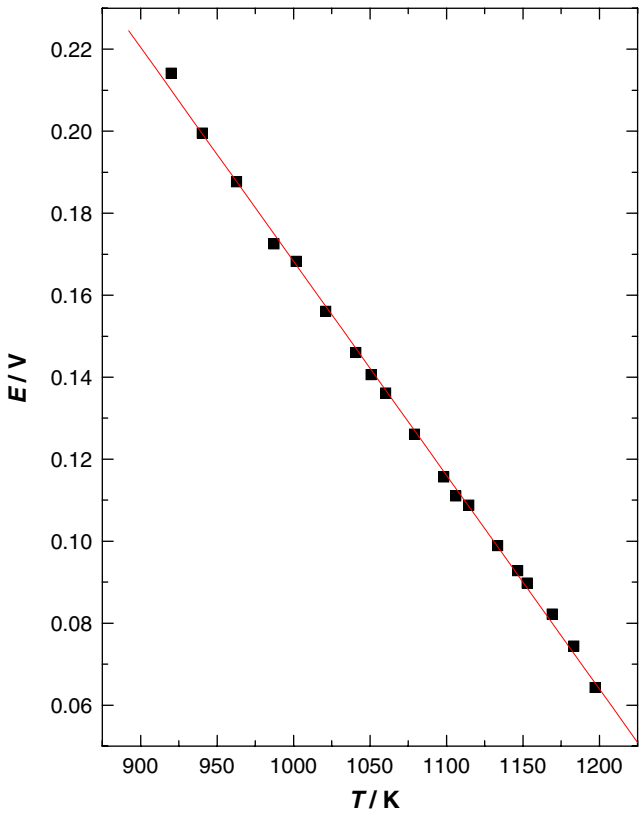

Fig. 2 Variation of e.m.f. of the cell $(-)\mathrm{Pt-Rh/\{YRhO_3(s)+Y_2O_3(s)+Rh(s)\}//CSZ//O_2\{}p(\mathrm{O_2})=21.21\ \mathrm{kPa}\mathrm{\}/Pt-Rh}(+)$ as a function of temperature

Table 1 Low-temperature standard molar heat capacity of $YRhO_3$(s)

T (K)	C_p (J K^{-1}mol^{-1})	T (K)	C_p (J K^{-1}mol^{-1})
126.9	45.2	211.8	83.1
132.6	50.4	218.0	85.4
138.6	54.4	224.2	87.6
144.7	57.6	230.4	89.6
150.6	60.2	236.6	91.4
156.6	62.6	242.8	93.0
162.7	64.8	249.0	94.4
168.8	66.9	255.3	95.8
174.9	69.0	261.5	97.0
181.0	71.2	267.8	98.1
187.1	73.6	274.0	99.4
193.3	75.9	280.3	100.4
199.4	78.4	286.5	101.1
205.6	80.8	292.8	101.9

Gibbs free energy of formation of $YRhO_3$(s) from elements in their standard state was determined as:

$$\Delta_f G^o\{YRhO_3(s)/\text{kJ mol}^{-1}(\pm 1.61)\} = -1147.4 + 0.2815\ T(\text{K}) \quad (11)$$

The error includes the standard deviation in e.m.f. and the uncertainty in the data taken from the literature. The Gibbs free energy of formation is a linear function of temperature within the investigated temperature range, i.e., from 920 to 1,197.3 K. The slope and intercept of this linear equation correspond, respectively, to the average values of the standard molar enthalpy and entropy of formation of $YRhO_3$(s) in the temperature range covered by e.m.f. measurement.

Standard molar heat capacity of $YRhO_3$(s)

The heat capacity values of $YRhO_3$(s) obtained in the two different temperature ranges: (1) $127 \le T$ (K)≤ 299 and (2)

Table 2 High-temperature standard molar heat capacity of $YRhO_3$(s)

T (K)	C_p (J K^{-1}mol^{-1})	T (K)	C_p (J K^{-1}mol^{-1})
305.0	103.9	485.6	115.8
326.8	105.4	505.5	116.7
346.3	107.0	525.4	117.7
365.9	108.3	545.4	118.3
385.6	110.2	565.4	118.9
405.6	112.0	585.4	119.4
425.7	112.8	605.4	120.3
445.8	114.0	625.5	121.1
465.7	115.0	645.6	121.9

Table 3 Derived thermodynamic functions of $YRhO_3$(s)

T (K)	$H^o_T - H^o_{298.15}$ (J mol^{-1})	C^o_p (J mol^{-1}K^{-1})	$S^o(T)$ (J mol^{-1}K^{-1})	fef[a] (J mol^{-1}K^{-1})
300.0	191	102.8	120.4	119.7
350.0	5,460	107.7	136.6	121.0
400.0	10,936	111.2	151.2	123.9
450.0	16,571	114.1	164.5	127.7
500.0	22,334	116.4	176.6	132.0
550.0	28,205	118.4	187.8	136.5
600.0	34,173	120.3	198.2	141.3
650.0	40,228	121.9	207.9	146.0
700.0	46,364	123.5	217.0	150.8
750.0	52,576	125.0	225.6	155.5
800.0	58,861	126.4	233.7	160.1
850.0	65,217	127.8	241.4	164.7
900.0	71,641	129.2	248.7	169.1
950.0	78,131	130.5	255.7	173.5
1,000.0	84,687	131.8	262.5	177.8

[a] fef $= -(G^o(T) - H^o(298.15\ \text{K}))/T$

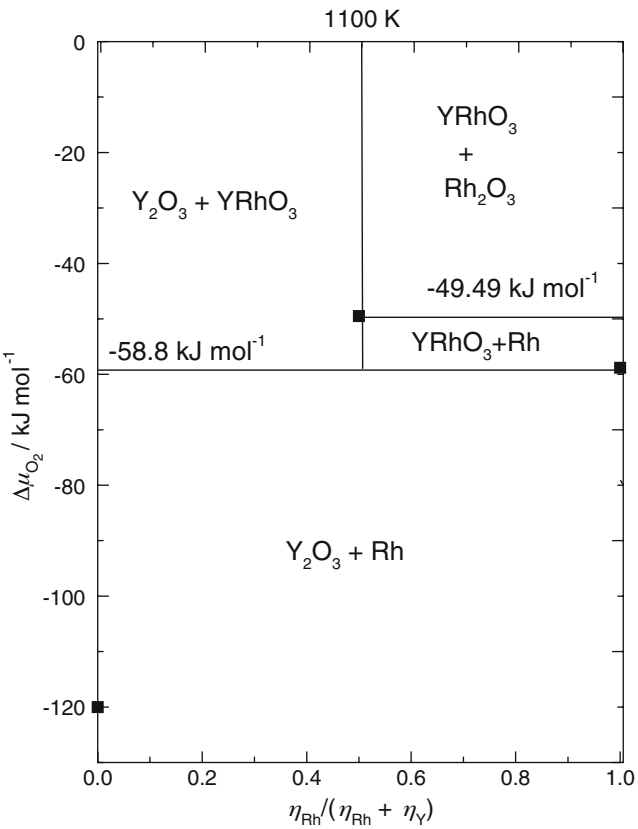

Fig. 3 Oxygen chemical potential diagram for the system Y–Rh–O at 1,100 K

$305 \leq T\,(\mathrm{K}) \leq 646$ are tabulated in Tables 1 and 2, respectively. The values of heat capacities are best fitted into the following polynomial expression in the higher temperature range by the least squares method.

$$C_p^{\circ}(\mathrm{YRhO_3,s},T)\left(\mathrm{J\,K^{-1}\,mol^{-1}}\right) = 109.838 + 23.181 \times 10^{-3} T(\mathrm{K}) - 12.596 \times 10^{5}/T^{2}(\mathrm{K}) \quad (12)$$

The heat capacity data for $YRhO_3$(s) at 298.15 K from the above equation were calculated to be 102.58 $\mathrm{Jmol^{-1}\,K^{-1}}$. The heat capacity at 298.15 K was also estimated in the present study by the Neumann–Kopp's rule [22], i.e., from the heat capacity data of the constituent binary oxides. Based on the heat capacity data of Rh_2O_3 and Y_2O_3(s) [21], the estimated heat capacity of $YRhO_3$(s) at 298.15 K was found to be 103.44 $\mathrm{Jmol^{-1}K^{-1}}$. As can be seen, there is good agreement between the estimated and calculated values. The heat capacity data for $YRhO_3$(s) have been reported for the first time.

Enthalpy and entropy of formation

The enthalpy of formation of $YRhO_3$(s) at 298.15 K has been calculated by the second law method. Heat capacity data obtained in this study by using a differential scanning calorimeter along with transition enthalpies of Rh(s) [23], Y(s), and O_2(g) [24], were used to determine the value of $\Delta_f H^{\circ}(\mathrm{YRhO_3,s,298.15\ K})$ and was found to be $-1{,}158.6$ kJ $\mathrm{mol^{-1}}$. From the heat capacity measurements and the entropy at the average experimental temperature, the standard molar entropy $S^{\circ}(298.15\ \mathrm{K})$ for this compound was calculated to be $S^{\circ}(\mathrm{YRhO_3,s,\ 298.15\ K}) = 119.7\ \mathrm{JK^{-1}\,mol^{-1}}$. Based on the calculated value of entropy and the measured heat capacity, the derived thermodynamic functions of $YRhO_3$(s) were calculated using the second law method, and the resulting values were extrapolated to 1,000 K and given in Table 3. It was assumed that in the temperature range from 646 to 920 K, there was no phase transition.

Oxygen potential diagram

In an isothermal oxygen potential diagram, the phase relations are represented as a function of partial pressure of oxygen. The oxygen potential diagram for the system Y–Rh–O at T=1,100 K, computed from the results of this study, is shown in Fig. 3. The composition variable is the cationic fraction $\eta_{\mathrm{Rh}}/(\eta_{\mathrm{Rh}}+\eta_{\mathrm{Y}})$, where η_i represents moles of component i. Oxygen is not included in the composition parameter. The diagram provides useful information on the oxygen potential range for the stability of various phases. The diagram is complementary to the conventional Gibbs triangle representation of phase relations in ternary systems, where the composition of each phase can be unambiguously displayed. All the topological rules of construction for conventional binary temperature–composition phase diagrams are applicable to the oxygen potential diagram shown in Fig. 3. When three condensed phases coexist at equilibrium in a ternary system such as Y–Rh–O, the system is bivariant; at a fixed temperature and total pressure, three condensed phases can coexist only at a unique partial pressure of oxygen. Therefore, horizontal lines on the diagram represent three phase equilibria [25]. Similar diagram at other temperatures can be readily computed from the thermodynamic data.

Conclusion

Yttrium rhodium (III) oxide was synthesized by the solid-state reaction route and characterized by X-ray diffraction method. The electromotive force was measured as a function of temperature using a solid-state electrochemical cell in the temperature range from 920.0 to 1,197 K. The Gibbs free energy of formation of $YRhO_3$(s) from elements in their standard state can be given by $\Delta_f G^{\circ}(\mathrm{YRhO_3},T,\mathrm{s})$ (kJ $\mathrm{mol^{-1}} \pm 1.61) = -1{,}147.4 + 0.2815\,T(\mathrm{K})$. Standard molar heat capacity of $YRhO_3$(s) is: $C^{\circ}{}_p(\mathrm{YRhO_3,s},T)(\mathrm{J\,K^{-1}\,mol^{-1}}) = 109.838 + 23.18 \times 10^{-3}\,T(\mathrm{K}) - 12.596 \times 10^{5}/T^{2}(\mathrm{K})$. The second law method gave the value of $\Delta_f H^{\circ}(\mathrm{YRhO_3,s,298.15\ K})$ and $S^{\circ}\{\mathrm{YRhO_3,s,\ 298.15\ K}\}$ as $-1{,}158.6$ kJ $\mathrm{mol^{-1}}$and 119.7 $\mathrm{JK^{-1}\,mol^{-1}}$, respectively. The Gibbs free energy of formation and the heat capacity of yttrium rhodium (III) oxide were determined and reported for the first time, and no other experimental data are available in the literature for comparison.

Acknowledgments The authors wish to thank Dr. N. D. Dahale, of FCD, BARC, for the XRD analysis. The authors are thankful to Dr. V. Venugopal, Group Director R C and I Group and Shri B. K. Sen, Head P.D.D., BARC, for their constant support and encouragement.

References

1. Hamberg I, Granquist CG (1986) J Appl Phys 60:123
2. Chopra KL, Major S, Pandya DK (1983) Thin Solid Films 102:1
3. Harris LA, Wilson RH (1978) Annu Rev Mater Sci 8:99
4. Ginley DS, Bright C (ed) (2000) MRS Bull 25(8)
5. Jarret HS, Sleight AW, Kung HH, Gillson JL (1980) J Appl Phys 51(7):3916
6. Ohta HT, Nomura K, Hiramatsu H, Ueda K, Kamiya T, Hirano M, Hosono H (2003) Solid State Electron 47:2261
7. Gysling HJ, Monnier JR, Appai G (1987) J Catal 103:407
8. Ohta HT, Orita M, Hirano M, Hosono H (2001) J Appl Phys 89:5720
9. Macquart R, Smith M, zur Loye HC (2006) Cryst Growth Des 6:1361

10. Mizoguchi H, Hirano M, Fujitsu S, Takeuchi T, Ueda K, Hosono H (2002) Appl Phys Lett 80:1207
11. Lazarev VB, Shaplygin IS (1978) Russ J Inorg Chem (Engl. Transl.) 23:1279
12. Shannon RD (1976) Acta Crystallogr A 32:751
13. Cruickshank KM, Glasser FP (1994) J Alloys Compd 210:177
14. Jacob KT, Okabe TH, Uda T, Waseda Y (1999) Bull Mater Sci 22:741
15. Kayanuma Y, Okabe TH, Mitsuda Y, Maeda M (2004) J Alloys Compd 365:211
16. Jacob KT, Waseda Y (2000) J Solid State Chem 150:213
17. Banerjee A, Prasad R, Venugopal V (2004) J Alloys Compd 381:58
18. Sabbah R, Xu-wu A, Chickos JS, Planas Leitao ML, Roux MV, Torres LA (1999) Thermochim Acta 331:93
19. Parida SC, Rakshit SK, Dash S, Singh Z, Prasad R, Venugopal V (2004) J Chem Thermodyn 36:911
20. Hohne GWH, Hemminger WF, Flammershein HJ (2003) Differential scanning calorimetry, 2nd edn. Springer, Berlin
21. Chase MW Jr (1998) JANAF thermochemical tables, 4th edn, (monograph no. 91995). ACS,AIP,NIST, Washington
22. Kubachewski O, Alcock CB, Spencer PJ (1993) Materials thermochemistry, 6th edn. Pergamon, Oxford
23. FactSage (1976–2004) Thermo-chemical database software, version 5.3.1—Thermfact. GTT Technologies, Germany
24. Graves K, Kirby B, Rardin R (1991) *FREED*., A free energy and enthalpy database manager, version 2.1
25. Pankratz LB (1982) Thermodynamic properties of elements and oxides. Bulletin 672, United States Bureau of Mines, Washington DC